

PHYSICS

Special Topic: Multiferroic Physics and Materials

Single-phase multiferroics: new materials, phenomena, and physicsChengliang Lu^{1,*}, Menghao Wu^{1,*}, Lin Lin^{2,*} and Jun-Ming Liu^{2,3}**ABSTRACT**

Multiferroics, where multiple ferroic orders coexist and are intimately coupled, promise novel applications in conceptually new devices on one hand, and on the other hand provide fascinating physics that is distinctly different from the physics of high- T_C superconductors and colossal magnetoresistance manganites. In this mini-review, we highlight the recent progress of single-phase multiferroics in the exploration of new materials, efficient roadmaps for functionality enhancement, new phenomena beyond magnetoelectric coupling, and underlying novel physics. In the meantime, a slightly more detailed description is given of several multiferroics with ferrimagnetic orders and double-layered perovskite structure and also of recently emerging 2D multiferroics. Some emergent phenomena such as topological vortex domain structure, non-reciprocal response, and hybrid mechanisms for multiferroicity engineering and magnetoelectric coupling in various types of multiferroics will be briefly reviewed.

Keywords: multiferroics, magnetoelectric coupling, non-reciprocity, topological domain structure, 2D multiferroics

INTRODUCTION

The terminology ‘multiferroics’ refers to those materials where more than one ferroic order, i.e. (anti)ferromagnetism, ferroelectricity, ferroelasticity, and ferrotoroidicity, coexist in one phase [1]. A combination of these multiple ferroic orders may allow intimate coupling among them, paving the way to realizing cross-control of various ordered parameters. The most striking of such controls is switching magnetization and/or ferroelectric polarization by electric and magnetic fields, as illustrated in Fig. 1. Nowadays, the term ‘multiferroics’ is often used specifically for those materials hosting ferroelectric and magnetic behaviors.

Multiferroics have been attracting enormous attention since the publication of the two seminal papers on TbMnO_3 and BiFeO_3 in 2003 [2,3]. So far, a large array of materials have been explored to show multiferroicity and magnetoelectric (ME) coupling, and these materials can be roughly classified into categories according to the microscopic mechanisms of ferroelectricity, noting that more than one mechanism may coexist in many cases. As proposed

by Khomskii, there are two types of multiferroics: type-I and type-II [4]. Type-II multiferroics, where ferroelectricity is generated in specific magnetic ordering, are sometimes called magnetism-driven multiferroics. All other single-phase multiferroics that do not have a magnetic origin of ferroelectricity can be categorized as type-I multiferroics. To more precisely capture the intrinsic physics, the type-I or type-II families can be further sub-classified according to the detailed microscopic mechanisms for ferroelectricity. This is rather meaningful, especially for type-I multiferroics. The double-layered magnetic perovskites exhibiting hybrid improper ferroelectricity represent an additionally developed sub-class of type-I multiferroics, which have shown highly designable multiferroicity in recent years [5,6].

In addition, while multiferroicity and ME coupling are most frequently discussed as bulk effects, 2D multiferroics and domain wall multiferroicity, which are so far less addressed but definitely appealing, have been revealed recently [7]. Even more, while realization of cross-controls of multiple ferroic orders, which offers routes to entirely new device architectures and may bring a revolution in

¹School of Physics & Wuhan National High Magnetic Field Center, Huazhong University of Science and Technology, Wuhan 430074, China;

²Laboratory of Solid State Microstructures, Nanjing University, Nanjing 210093, China and ³Institute for Advanced Materials, Hubei Normal University, Huangshi 435002, China

***Corresponding**

authors. E-mails:

cllu@hust.edu.cn;

wmh1987@hust.edu.cn;

nj-qm@nju.edu.cn

Received 9 May

2019; **Revised** 15

June 2019; **Accepted**

20 June 2019

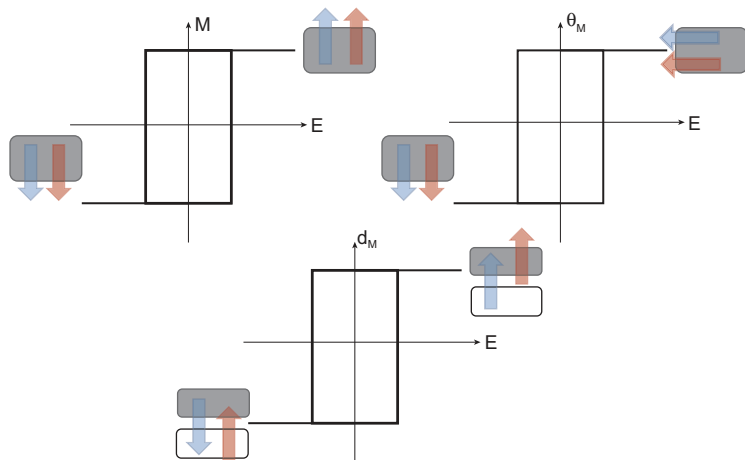


Figure 1. Three types of ME coupling: reversal of net magnetization M upon ferroelectric switching; change of magnetic easy axis upon ferroelectric switching; change of magnetic distribution upon ferroelectric switching in 2D bilayer systems. Red and blue arrows denote the polarization and magnetization directions, respectively. θ_M and d_M respectively denote the angle of the magnetic easy axis and the center coordinate of magnetic dipoles.

information processing and storage, has been the main stream of multiferroic research, a number of fascinating phenomena not in the main stream but sufficiently compelling, such as non-reciprocity [8,9], topological orders [10], and thermal Hall effects [11], have been discovered in multiferroic materials. These events allow distinctive functionalities beyond the ME coupling and moisturize multiferroic research.

Concomitant with progress in this highly interdisciplinary field, quite a few review articles on various aspects of multiferroics and underlying physics are available [12–16]. The continuous enthusiastic endeavors on multiferroics have gradually moved this promising discipline into a new era. Especially in the past five years, distinctly different and appreciated multiferroic mechanisms beyond the well-known ones and a series of new phenomena have been observed in several alternative systems, largely extending the essence and scope of multiferroicity. In the present mini-review, we give an overview of the recent advances in three aspects: single-phase materials, emerging phenomena, and updated physical scenarios. We certainly do not make any attempt to cover everything in this short article, and the topics chosen are more or less biased by the authors' own research interests. The review is organized according to the classification of multiferroics, and only those advances in recent several years in this framework will be discussed.

TYPE-I MULTIFERROICS

First of all, BiFeO_3 is an unavoidable material if one discusses type-I multiferroics where ferroelectricity

and magnetism are believed to originate from two different cations; i.e. the 6s lone pair electrons of Bi give rise to ferroelectricity and the 3d-electrons of Fe lead to canted G-type antiferromagnetic (AFM) order [3]. This represents a major strategy that was initially utilized to 'produce' type-I multiferroics, and a variety of Bi-based and Pd-based type-I systems have been synthesized and characterized [17]. An extension of this strategy in concomitance with research progress is exemplified by EuTiO_3 where the 4f magnetic moment of Eu and d^0 -ferroelectricity of Ti coexist, and are efficiently coupled under some specific conditions [18].

Hexagonal manganites RMnO_3 (h- RMnO_3 where R is a rare-earth element or Y, In) serve as another class of materials to obtain type-I multiferroicity, with route in the line of geometric frustration. The buckling of layered MnO_5 polyhedra that form the in-plane triangle geometry causes the collective movements of Y^{3+} along the c -axis with a two-up-one-down profile, leading to the c -axis net electric polarization [19]. Since geometrical frustration is essential in generating ferroelectricity, h- RMnO_3 is also called a geometric multiferroic. A signature of these geometric multiferroics is that both ferroelectricity and magnetism are closely linked to structural distortion, which may promise evident ME coupling through the spin–lattice mechanism. Direct evidence for this is the coupled ferroelectric and magnetic domains in h- YMnO_3 , as observed using the second harmonic generation [20].

An emerging phenomenon with h- RMnO_3 is the identification of a unique structurally and ferroelectrically coupled domain structure where six domains in the $[\alpha^+, \gamma^-, \beta^+, \alpha^-, \gamma^+, \beta^-]$ sequence meet at the conjunct point, constituting the six-fold vortex or antivortex [21]. Each six-fold degenerate vortex pairs with one antivortex and these pairs occupy the whole space, resulting in a topologically non-trivial vortex–antivortex domain structure. The ME coupling mediated by lattice instability at domains and walls can be directly captured using the ME force microscopy technique [22]. In fact, the topological domain structure can further be manipulated by electric field [23,24], stiffness anisotropy [25], and self-poling resulting from oxygen off-stoichiometry [26], as shown in Fig. 2, and also in thin films [27]. The six-fold topological domain pattern may be protected by the so-called $Z_2 \times Z_3$ symmetry in h- RMnO_3 , essentially determined by the trimerized tilting of MnO_5 bipyramids [10], while two-, four-, and eight-fold vortex configurations due to different topological defects have been observed [28], also shown in Fig. 2. Such topological domain patterns are not limited to h- RMnO_3 but are evidenced in other materials such as BiFeO_3 [29]. More information can be found in an excellent topic review by

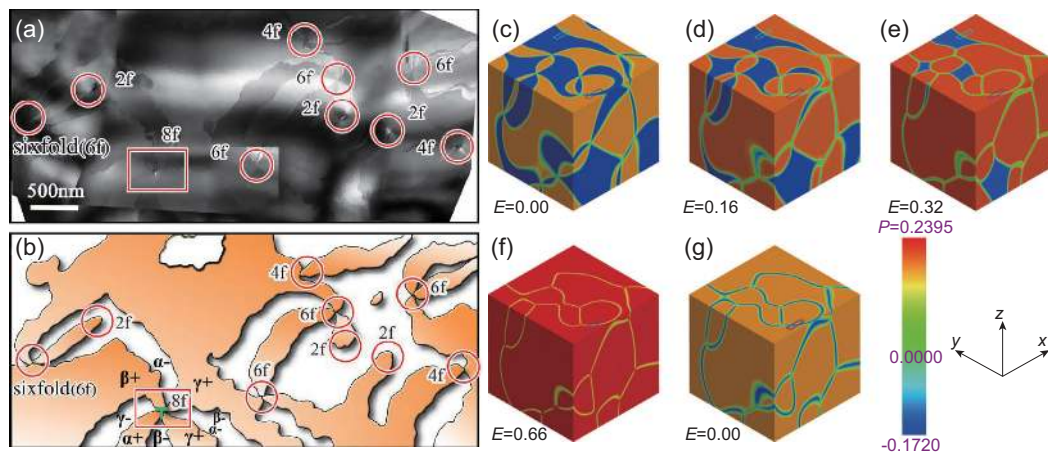


Figure 2. Six-fold and non-six-fold vortex domains in hexagonal YMnO_3 single crystals: (a) Identified with mesoscale dark-field transmission microscopy, and (b) the corresponding schematic diagram [28]. (c)–(g) illustrate the simulated 3D topological domains manipulated with electric field. The magnitude of ferroelectric polarization is scaled by the color bar [23].

Huang and Cheong [10]. In addition, it should be mentioned that the hexagonal structure can be transformed to an orthorhombic one via chemical and strain engineering, and then totally different multiferroicity and ME coupling may be obtained, while orthorhombic RMnO_3 exhibits type-II multiferroic behaviors, to be illustrated in the section entitled ‘Type-II multiferroics’.

The scenario of geometrically driven multiferroicity is also applicable to other iso-structural compounds, e.g. RFeO_3 [30–32]. Unlike h-RMnO_3 , hexagonal RFeO_3 (h-RFeO_3) is not as stable as orthorhombic RFeO_3 , but the energy difference between them is small, suggesting the possibility of hexagonal \leftrightarrow orthorhombic transformation triggered by small external stimuli. For example, h-RFeO_3 structure can be easily obtained in thin films via the substrate matching route. Indeed, elevated temperature ferroelectricity in $(\text{Lu}, \text{Yb}, \text{Tm})\text{FeO}_3$ epitaxial films has been demonstrated and the measured remnant polarization $P_r \sim 5 \mu\text{C}/\text{cm}^2$ [33,34], as shown in Fig. 3. In the meanwhile, switchable ferroelectric photovoltaic effects were revealed in h-RFeO_3 , in analogy to multiferroic BiFeO_3 . Chemical doping is another useful route to achieve a hexagonal phase. Surprisingly, the hexagonal phase can be stabilized by chemical doping at the R-site with a small R-ionic size. One case is $(\text{Lu}, \text{Sc})\text{FeO}_3$ [35], noting that h-LuFeO_3 is nevertheless chemically unstable. The first-principles calculations on the $(\text{Lu}, \text{Sc})\text{FeO}_3$ solid solution suggested that the hexagonal phase is lower in energy than the orthorhombic phase. This finding is expected to promote efforts to synthesize high-quality h-LuFeO_3 bulk crystals, once a great challenge. The similar geometric ferroelectricity in h-RFeO_3 and h-RMnO_3 hints at the existence of topological domain structure in h-RFeO_3 [31,36].

In comparison with h-RMnO_3 , h-RFeO_3 commonly shows much higher antiferromagnetic Néel temperature T_N , appreciated for multiferroic applications. Although the underlying physics remains elusive, the strong Fe–Fe exchange and lattice distortion should be the pivotal ingredients [37], as also found by Sinha *et al.* that T_N has a nearly linear dependence on the tolerance factor, suggesting a connection with the polar distortion [38], as shown in Fig. 3. These results offer an efficient strategy to modulate the multiferroic properties via structural engineering.

The final class of type-I multiferroics, which was discovered long ago but recently addressed once more, is fluorides, BaMF_4 ($M = \text{Mn}, \text{Ni}, \text{Co}, \text{Fe}, \text{Cu}$) [39–41]. The ferroelectricity is believed to originate from the collective rotation of MF_6 octahedra, and transition metals provide magnetism. The ferroelectric Curie temperature in some fluorides can be high, even exceeding 1000 K and the melting point. However, the AFM ordering usually emerges at a much lower temperature, typically $T_N < 50$ K. It should be mentioned that multiferroic fluorides have been less addressed as compared with other type-I multiferroics, perhaps due to the difficulties in synthesis of high-quality materials and electric characterization. In addition, strong room-temperature blue–violet photoluminescence in BaMnF_4 was found very recently [42], a surprising functionality in multiferroic fluorides.

TYPE-II MULTIFERROICS

For type-II multiferroic materials, electric polarization is believed to be generated by a specific magnetic order, allowing a remarkable ME response. It was initially discovered in orthorhombic RMnO_3

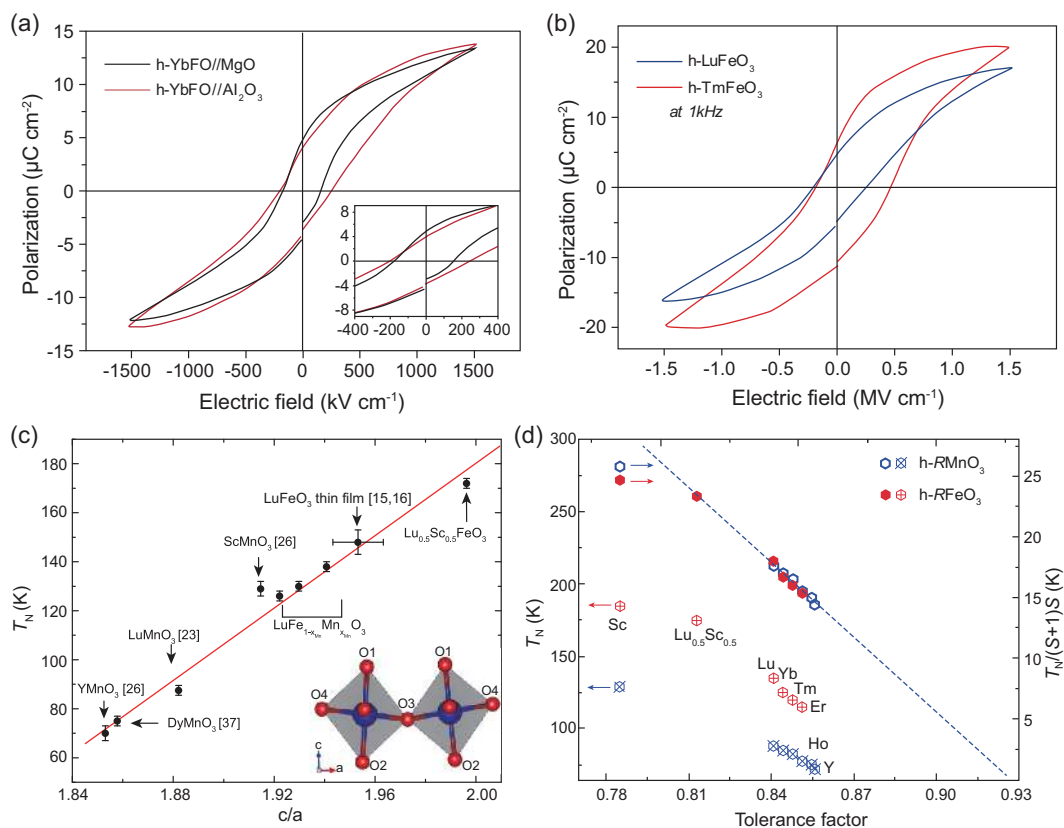


Figure 3. Room-temperature ferroelectric hysteresis loops of (a) hexagonal YbFeO₃ films grown on different substrates, and (b) hexagonal LuFeO₃ and TmFeO₃ films grown on Al₂O₃ (0001) substrates [33,34]. Antiferromagnetic transition temperature T_N as a function of (c) lattice parameter c/a , and (d) tolerance factor for hexagonal manganites and ferrites [37,38]. In (d), $T_N/(S+1)S$ as a function of tolerance factor is also plotted, in which S means the spin on Fe.

[2] and RMn₂O₅ [43], and subsequently dozens of materials have been found to show type-II multiferroicity. Three microscopic mechanisms, i.e. the inverse Dzyaloshinskii–Moriya (DM) interaction, exchange striction, and spin-dependent p - d hybridization, have been proposed [12,14]. In particular, for materials hosting spiral spin order (SSO), the electric polarization can be sharply and completely flipped from one direction to another, resulting in remarkable ME response, although the inverse DM interaction-induced polarization is generally small ($<0.01 \mu\text{C}/\text{cm}^2$) [2]. In contrast, the exchange-striction-induced electric polarization, most likely observed in materials with collinear spin order, can be much larger ($>0.1 \mu\text{C}/\text{cm}^2$), and even comparable with conventional ferroelectrics [44,45]. Recently, a giant polarization of $P \sim 2 \mu\text{C}/\text{cm}^2$ in RMnO₃ under pressure, due to exchange striction, was demonstrated [46–48]. It should be mentioned that the ME coupling in multiferroics dominated by the exchange striction mechanism is usually not as striking as that in multiferroics of spiral spin order, and polarization switching usually requires a relatively high magnetic field. It is noticed

that the spin-dependent p - d hybridization mechanism is found only in several materials although a unique ME coupling mode that the electric polarization can be successively rotated by magnetic field has been observed [49].

The past five years have seen the appearance of many more type-II multiferroics; it would be impossible to mention all of them, but several examples are described below.

- (1) Aeschynite-type polar magnets RFeWO₆ that possess multiferroicity with spontaneous polarization $P \sim 3 \mu\text{C}/\text{m}^2$ below ~ 20 K, arising from an unusual commensurate and non-collinear magnetic configuration of Fe³⁺ [50]. Further theoretical calculations revealed a polarization as large as $\sim 7.5 \mu\text{C}/\text{cm}^2$, likely accessible in single crystals.
- (2) Tungstate LiFe(WO₄)₂ with a wolframite structure. A polarization of $\sim 10 \mu\text{C}/\text{m}^2$ due to non-collinear magnetism of Fe³⁺ in polycrystalline samples below ~ 20 K was reported [51]. The spiral spin order-driven multiferroicity looks highly sensitive to structural variations, noting that NaFe(WO₄)₂ is non-multiferroic in spite

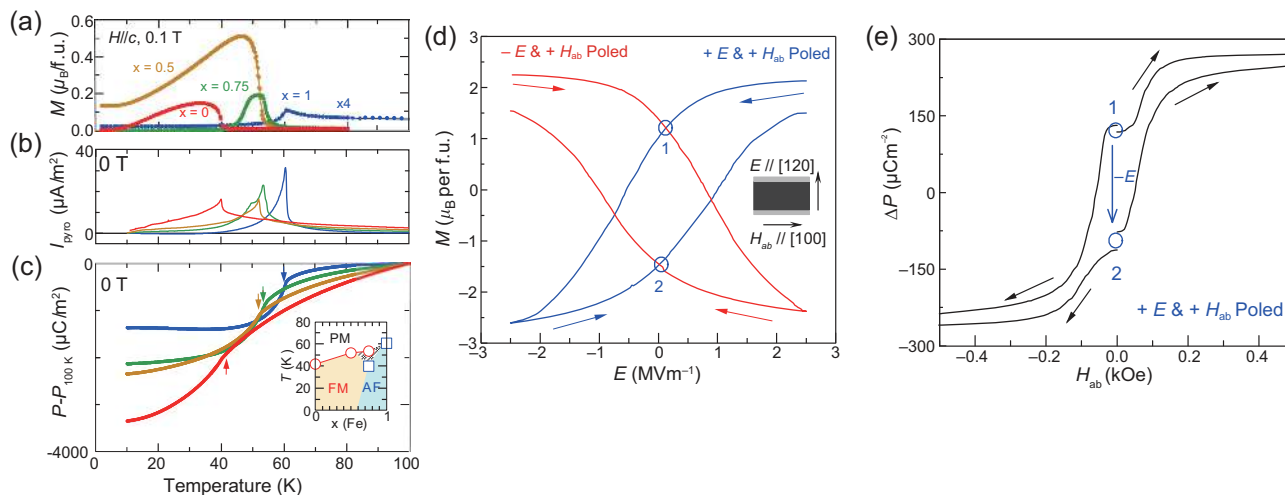


Figure 4. Temperature dependence of (a) magnetization, (b) pyroelectric current, and (c) time-integrated change of polarization from that at $T = 100$ K in multiferroic $(\text{Mn}_{1-x}\text{Fe}_x)_2\text{Mo}_3\text{O}_8$ [62]. In the inset of (c), a summarized phase diagram is presented, in which the open circles and squares are estimated transition temperatures. (d) Electric reversal of magnetization, and (e) P -variation as a function of magnetic field at $T = 10$ K in hexaferrite $\text{Ba}_{0.4}\text{Sr}_{1.6}\text{Mg}_2\text{Fe}_{12}\text{O}_{22}$ [81].

of its similarity to $\text{LiFe}(\text{WO}_4)_2$ in composition and stoichiometry but its difference from $\text{LiFe}(\text{WO}_4)_2$ in crystallographic structure. The high sensitivity to lattice structure suggests spin–lattice coupling as the possible mechanism for the distinctive ME controls.

- (3) Vanadate $\text{M}_2\text{V}_2\text{O}_7$, another family that was found to show type-II multiferroicity. In $(\text{Ni}, \text{Co})_2\text{V}_2\text{O}_7$, two multiferroic phases were respectively identified at low and high magnetic field regions, while a non-ferroelectric phase in between them with a half-magnetization plateau was observed [52]. These observations are similar to the measured results on $\text{Ni}_3\text{V}_2\text{O}_8$ and MWO_4 , and the existence of multiple multiferroic phases may be utilized for unusual ME memory applications [53,54].
- (4) A long list of other type-II multiferroics, including $\alpha\text{-NaFeO}_2$ [55], Mn_2O_3 [56], $(\text{La}, \text{Bi})\text{Mn}_3\text{Cr}_4\text{O}_{12}$ [57,58], Ni_3TeO_6 [59,60], $(\text{Fe}, \text{Mn})_2\text{Mo}_3\text{O}_8$ [61–63], $\text{Co}_4\text{Nb}_2\text{O}_9$ [64], Mn_2MnWO_6 [65], $\text{RFe}_3(\text{BO}_3)_4$ [66–68], $\text{KCu}_3\text{As}_2\text{O}_7(\text{OD})_3$ [69], $\text{NaFeSi}_2\text{O}_6$ [70], $\text{In}_2\text{NiMnO}_6$ [71], and so on. Certainly, this list should not exclude materials other than oxides, and compounds with other anions such as S and Se have been revealed to show type-II multiferroicity too, including CaOFeS [72], MnSb_2S_4 [73], BaFe_2Se_3 [74], $\text{Cu}_3\text{Bi}(\text{SeO}_3)_2\text{O}_2\text{Cl}$ [75], CsCuCl_3 [76], and CuBr_2 [77].

Although the physics of most type-II multiferroics can be understood within the framework of these three mechanisms, there are exceptions, at least qualitatively. One exception is $\text{LaMn}_3\text{Cr}_4\text{O}_{12}$,

a system with cubic quadruple perovskite structure and collinear spin alignment, and the spin-driven ferroelectricity cannot be ascribed to any of the three mechanisms [58]. A scenario composed of spin-orbit coupling and dual G-type AFM ordering was proposed to interpret the multiferroicity. Apart from this, it was demonstrated that both ferroelectric polarization and ME coupling can be significantly enhanced if La is replaced by the well-known ferroelectric active cation Bi^{3+} . $\text{BiMn}_3\text{Cr}_4\text{O}_{12}$ provides a rare example with joint multiferroicity in the same phase [57]. Spin-ice pyrochlores such as $\text{Ho}_2\text{Ti}_2\text{O}_7$ and $\text{Dy}_2\text{Ti}_2\text{O}_7$, highly noted for their unusual finite zero-point entropy and magnetic monopoles, were recently found to host multiferroicity and ME coupling, which probably has a spin-related mechanism [78–80].

Despite these advances in the past two decades, indomitable effort in searching for more compounds with desirable performance is still underway. Room-temperature multiferroicity, sufficient ME response, and ferromagnetism, as well as electro-control of magnetization, remain the major concerns. One may find that antiferromagnetism and spin-driven ferroelectricity look like the two sides of a coin for type-II multiferroics. Regarding this, building up a ferromagnetic lattice seems to be a promising route to have evident net magnetization, accessed in the $\text{M}_2\text{Mo}_3\text{O}_8$ family where sizeable macroscopic magnetization $\sim 0.5 \mu_B/\text{f.u.}$ and ferroelectric polarization as large as $\sim 0.2500 \mu\text{C}/\text{cm}^2$ have been measured [62], as shown in Fig. 4. The electrically driven reversal of a large magnetization of $\sim 2.0 \mu_B/\text{f.u.}$ in Y-type hexaferrite $\text{Ba}_{0.4}\text{Sr}_{1.6}\text{Mg}_2\text{Fe}_{12}\text{O}_{22}$ was identified, accompanied with a giant ME coefficient

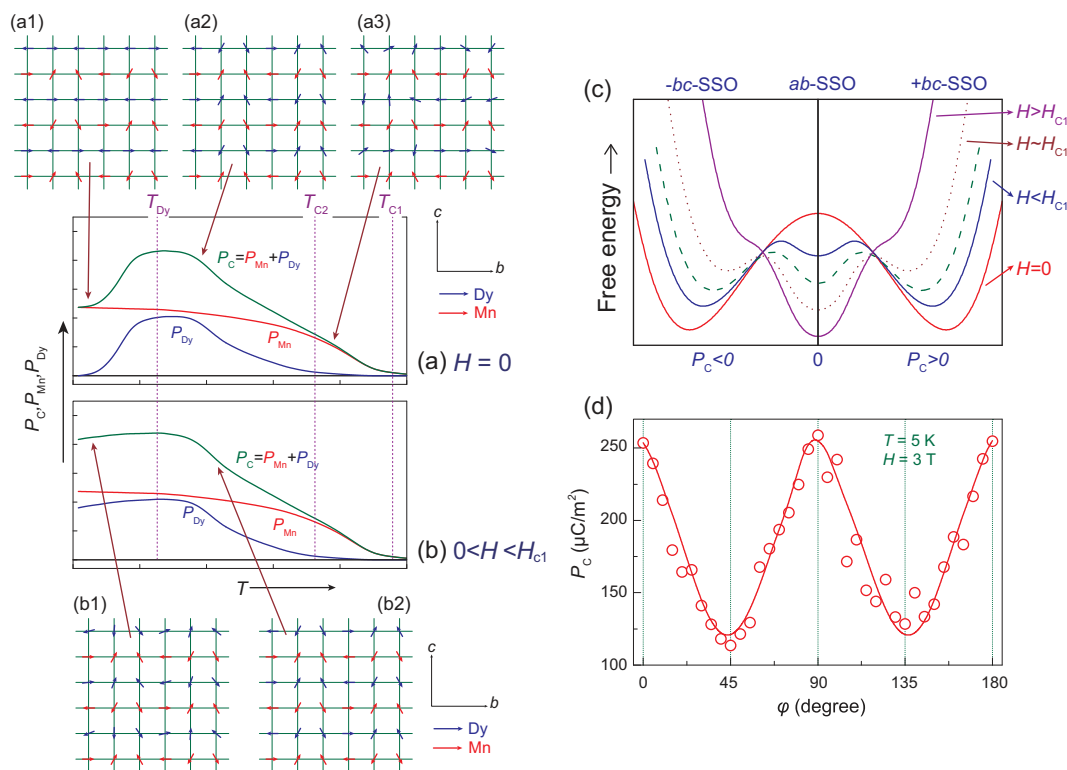


Figure 5. Schematics of the dual nature of multiferroicity in orthorhombic DyMnO_3 . (a) At $H = 0$, $P_{\text{Mn}} \sim S_{\text{Mn}} \times S_{\text{Mn}}$ arises at T_{C1} , and then $P_{\text{Dy}} \sim S_{\text{Dy}} \cdot S_{\text{Mn}}$ emerges at T_{C2} due to the Dy–Mn exchange striction. Below T_{Dy} , P_{Dy} is diminished with the onset of an independent Dy spin order. (b) With $H < H_{\text{C1}}$ (before the flip transition of the spiral plane), P_{Dy} can be recovered due to the re-emergence of Dy–Mn coherence. (c) Sketch of an energy diagram of P -switching and the corresponding spin-spiral plane in DyMnO_3 , which can be tuned by the application of H . (d) Continuous magnetoelectric control in DyMnO_3 films with twin-like domains, which can be qualitatively understood using the energy diagram shown in (c) [85].

$\sim 33\,000 \text{ psm}^{-1}$ [81], as shown in Fig. 4 too. Theoretically, near-room-temperature tunable ferromagnetism and electric polarization as large as $\sim 10 \mu\text{C}/\text{cm}^2$ in R_2NiMnO_6 superlattices have been predicted, definitely deserving experimental exploration [82].

As stated earlier, the inverse DM interaction can generate a remarkable ME response, while the exchange striction can provide large electric polarization. It has been a long-standing issue to combine the two mechanisms concurrently in the same system. This issue was once investigated taking orthorhombic DyMnO_3 as an example. It was proposed that the electric polarization consists of two components, including component $P_{\text{Mn-Mn}}$ due to the inverse DM interaction with Mn^{3+} spiral spin order and component $P_{\text{Dy-Mn}}$ due to the $\text{Dy}^{3+}\text{-Mn}^{3+}$ exchange striction [83–88], as illustrated in Fig. 5. Component $P_{\text{Mn-Mn}}$ can be flipped by magnetic field H from one direction (i.e. the c -axis) to another (i.e. the a -axis). Importantly, component $P_{\text{Dy-Mn}}$ rigidly tracks component $P_{\text{Mn-Mn}}$, and thus remarkably enhances the total electric polarization and ME effect. We may call this behavior the hybrid mechanism. In addi-

tion, if a twin-like structural domain structure is involved in DyMnO_3 thin films, a distinctive continuous ME control has been observed [85], as shown in Fig. 5 too. Such a hybrid mechanism is not limited to DyMnO_3 but is broadly available in the orthorhombic RMnO_3 family, representing another efficient roadmap to enhance the multiferroicity and ME coupling. Usually, this hybrid mechanism requires more than one magnetic cation, such as Dy and Mn in DyMnO_3 , compatible with the scenario of magnetism enhancement in a ferrimagnetic lattice.

Besides good materials for multiferroicity, emergent phenomena discovered in type-II multiferroics are also receiving attention. For example, non-reciprocity and the thermal Hall effect observed in some multiferroics are indeed compelling [8,9]. The non-reciprocal effect means that the motion of an object such as an electron, magnon, phonon, and light in one direction is different from that in the opposite direction, like the diode effect. The crucial physical ingredient for a non-reciprocal effect is broken inversion symmetry. In the case of multiferroics, both time reversal and space inversion symmetries are broken, and thus non-reciprocal directional

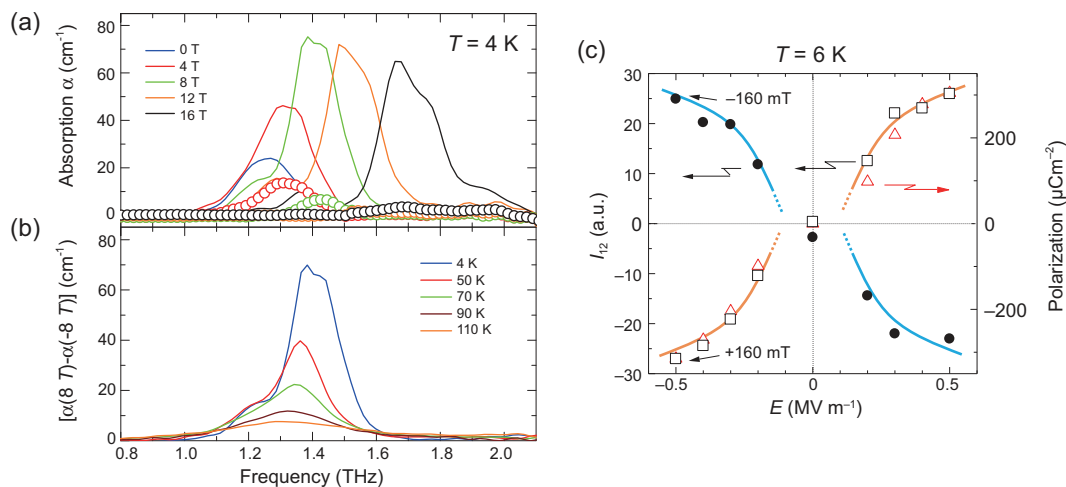


Figure 6. (a) and (b) present the remarkable difference of absorption coefficient for positive (solid lines) and negative (open circles) magnetic fields in $(\text{Fe}_{0.6}\text{Zn}_{0.4})_2\text{Mo}_3\text{O}_8$ [91]. (c) Non-reciprocal microwave response in a multiferroic helimagnet $\text{Ba}_2\text{Mg}_2\text{Fe}_{12}\text{O}_{22}$ [93]. The integrated intensities of non-reciprocity I_{12} can be reversed by an external electric field at $T = 6$ K, consistent with the P -switching behavior (open triangles).

dichroism/birefringence can in principle be widely observed. For instance, one-way transparency of light was revealed in multiferroic CuBO_2 [89], and magnetic switching of light transmission was identified in $(\text{Cu}, \text{Ni})\text{B}_2\text{O}_4$ [90]. In $\text{FeZnMn}_3\text{O}_8$, a giant terahertz optical diode effect was reported even in the paramagnetic phase [91], as shown in Fig. 6. In fact, a room-temperature optical diode effect due to the spin-current-driven dynamic ME coupling was demonstrated in BiFeO_3 [92]. More interestingly, the non-reciprocal microwave response in multiferroic helimagnet $\text{Ba}_2\text{Mg}_2\text{Fe}_{12}\text{O}_{22}$ can be reversed by an electric field [93], as shown in Fig. 6 too. While these investigations have illustrated the tantalizing aspects of non-reciprocity in multiferroics, more investigations are desired to exploit the full merit of this effect, such as efficient controls of the significantly large non-reciprocal response by means of an electric/magnetic field above room temperature, and readers may refer to two recent topic review papers [8,9].

Type-II multiferroics (especially those dominated with the exchange striction mechanism) usually show strong spin–lattice coupling, which guarantees the cross-control of phonons (spin excitations) by a magnetic field (electric field). The thermal Hall effect is one typical example, in which the heat flow dominated by phonons can be deflected by a perpendicular magnetic field. Unlike charged particles or quasi-particles, the phonon is neutral. In $(\text{Zn}_x\text{Fe}_{1-x})_2\text{Mo}_3\text{O}_8$, a giant thermal Hall effect $k_{xy} \sim 30 \times 10^{-3} \text{ W K}^{-1} \text{ m}^{-1}$ was observed, making an effective probe for spin–lattice coupling and magnetic control of thermal currents possible [11]. Certainly, one may ask how a thermal Hall effect can be effec-

tively modulated electrically, and whether the flow of phonons possesses any non-reciprocal response.

HYBRID IMPROPER MULTIFERROICITY IN DOUBLE-LAYERED PEROVSKITES

It is still not very clear what the third road is, in addition to type-I and type-II multiferroics, considering the fact that none of these materials can meet all requirements for multiferroicity. Nevertheless, improper ferroelectrics with magnetic species seem to be very interesting recently. For perovskites ABO_3 , rotation and tilting of BO_6 octahedra can be ubiquitously observed if the tolerance factor is small. This is a kind of antiferrodistortion (AFD) mode, leading to a local charge dipole associated with the bent B–O–B bonds.

Unfortunately, such local charge dipole in these simple perovskites would be compensated by the neighboring BO_6 layers, resulting in zero net electric polarization, as often observed. An extension of this scenario towards double-layered perovskites $\text{A}_3\text{B}_2\text{O}_7$ would make the story different. Here, a combination of two AFD modes would generate an improper electric polarization [5], already demonstrated in a large array of compounds such as $\text{Ca}_3\text{Ti}_2\text{O}_7$ [6,94,95], $\text{Ca}_3\text{Mn}_2\text{O}_7$ [96], and the $(1-x)(\text{Ca}_{0.6}\text{Sr}_{0.4})_{1.15}\text{Tb}_{1.85}\text{Fe}_2\text{O}_7-(x)\text{Ca}_3\text{Ti}_2\text{O}_7$ series [97] etc., as shown in Fig. 7. In this sense, improper magnetic ferroelectric compounds, tentatively called hybrid improper multiferroics, offer opportunities with which one may find some good multiferroics. Surely, one may argue that this two-mode combination is similar to the physics of type-I

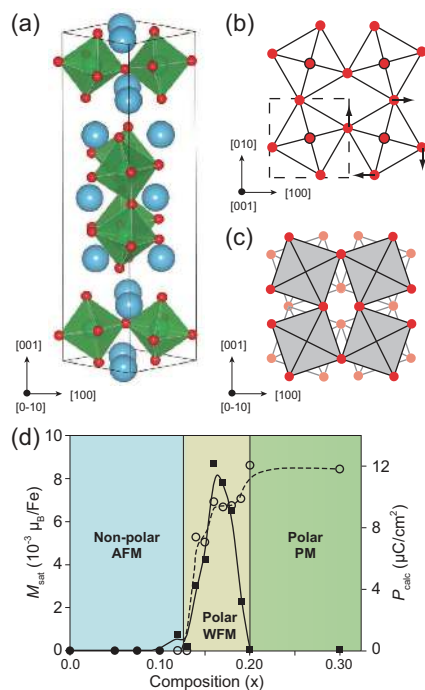


Figure 7. (a) Crystal structure of double-layered perovskite $A_2B_3O_7$ showing octahedral tilting and rotation. Two different antiferrodistortive modes: (b) the X_2^+ rotation mode, and (c) the X_3^- tilt mode [5]. (d) Phase diagram of $(1-x)(Ca_{0.6}Sr_{0.4})_{1.15}Tb_{1.85}Fe_2O_7-(x)Ca_3Ti_2O_7$ at $T = 300$ K [97]. Solid squares: measured saturated magnetization. Open circles: calculated polarization.

multiferroics where ferroelectricity and magnetism have separate origins. The striking feature of these hybrid improper multiferroics is that ferroelectricity and magnetism arise from the same cation, allowing prominent ME control via spin–lattice coupling.

Hybrid improper multiferroics show at least three advantages, evidenced in several double-layered perovskites. First, both ferroelectric and magnetic transition may occur above room temperature, pivotal for potential applications. Weak ferromagnetism and polar phase were revealed above $T \sim 300$ K in $(1-x)(Ca_{0.6}Sr_{0.4})_{1.15}Tb_{1.85}Fe_2O_7-(x)Ca_3Ti_2O_7$ with $0.1 < x < 0.2$ [97]. Second, double-layered perovskites $A_3B_2O_7$ are highly designable by simple chemical consideration. Both the A-site and B-site can be occupied by either different cations or cation groups, providing a broad platform to engineer the physical properties on purpose. Third, multiferroicity in $A_3B_2O_7$ is simply due to structural distortion; i.e. a combination of non-polar rotation of BO_6 octahedra induces net electric polarization. Along this line, a natural proposal to tailor the multiferroicity of $A_3B_2O_7$ is thin film epitaxy. An ultra-low coercive field for ferroelectric switching was identified in $Ca_3Ti_2O_7$ epitaxial films, although

the bulk counterpart shows a huge coercivity ~ 200 kV/cm [98].

A more interesting concept along this way is an integration of the type-II mechanism into hybrid improper multiferroics. Because of the clear advantages of the $A_3B_2O_7$ family for highly tunable chemical compositions, comprehensive chemistry engineering makes it possible to design special magnetic configurations that could generate type-II multiferroicity. In this sense, to simultaneously obtain good ferroelectricity, giant ME coupling, and high ferroelectric/magnetic transition temperatures in a single material seems to be beyond a dream.

OTHER SINGLE-PHASE MULTIFERROICS

While type-I, type-II, and hybrid improper multiferroics represent the three main streams, there are also many brooks that may not be significant but are interesting. We highlight several cases without losing the generality.

First, a common perception assumes that a ferroelectrically active cation has to follow the d^0 -rule. As an exception, non- d^0 Mn-driven ferroelectric displacement was initially proposed in antiferromagnetic $BaMnO_3$ [99], and subsequently demonstrated in $Sr_{1-x}Ba_xMnO_3$ [100] and $SrMnO_3$ [101]. The non- d^0 ferroelectricity originates a spontaneous off-center displacement of Mn, arising from a second-order Jahn–Teller distortion. In $Sr_{0.5}Ba_{0.5}MnO_3$, room-temperature ferroelectricity was evidenced, and a large spontaneous polarization $\sim 4.5 \mu C/cm^2$ was obtained at $T = 2$ K (which could be triple as the sample is single-domain) [100]. In strained $SrMnO_3$ thin films, a well-defined ferroelectric hysteresis loop with a gigantic remnant polarization of $\sim 55 \mu C/cm^2$ at $T = 10$ K was reported very recently [101].

Second, theoretical works have suggested that the non- d^0 Mn-driven multiferroicity is highly tunable. A rich multiferroic phase diagram was proposed in strained $SrMnO_3$ thin films, and coexistence of ferromagnetism and ferroelectricity was found as the strain was above $\sim 4\%$ [102]. By replacing Sr with Ba in strained thin films, a first-order magnetic transition, i.e. from the AFM state with smaller polarization to the ferromagnetic state with larger polarization, was predicted [103]. Subsequently, the *ab initio* calculations predicted a strain-induced morphotropic phase boundary (MPB) in $Sr_{0.5}Ba_{0.5}MnO_3$ thin films accommodating giant ME coupling and magneto-striction [104]. The multiferroicity due to the non- d^0 cation off-center displacement was observed in super-tetragonal $BiFeO_3$, and scanning transmission

electron microscopy imaged a relative displacement between Fe and Bi ions as large as $\sim 0.33 \text{ \AA}$ [105]. Such a super-tetragonal phase can be switched to rhombohedral phase, suggesting a striking modulation of physical properties [106]. In addition, perovskite RCrO_3 (and probably the RCrO_4 family) represents another group of multiferroics that show ferroelectricity due to the non- d^0 cation off-center displacement, and this topic is nevertheless much less addressed [107,108]. These findings also suggest structural instability in non- d^0 cation oxides if the cation–O–cation bond is largely elongated, favoring an off-center displacement. This scenario resembles conventional ferroelectrics, thus hinting at two possibilities for non- d^0 multiferroicity: high strained epitaxy and negative chemical pressure with a big A-site cation, as exemplified in $\text{Sr}_{0.5}\text{Ba}_{0.5}\text{MnO}_3$ [100].

Third, there are more materials that have been demonstrated to possess multiferroicity but the underlying mechanism remains elusive. For instance, $\varepsilon\text{-Fe}_2\text{O}_3$ was theoretically proposed to show room-temperature multiferroicity with coexisting ferrimagnetism and ferroelectricity [109]. Room-temperature ferroelectricity and ferromagnetism were identified in $\text{SrFeO}_{2.5}$, probably due to the displacement of ions and rotation of tetrahedra [110]. In fact, even for those multiferroics whose properties are believed to be well understood, some unexpected phenomena are often observed if a more detailed investigation is carried out. One example is GdMn_2O_5 , a member of the intensively studied RMn_2O_5 family, and the multiferroicity can be notably tuned by electric field poling in the paraelectric phase, an amazing fact to be understood [111].

2D MULTIFERROICS

Dimensionality is a well-accepted and promising concept that often makes major impact on materials properties and underlying physics. This concept is also significant for multiferroics, and thus 2D magnetism and ferroelectricity have been investigated recently. The existence of 2D ferromagnetism represents a major breakthrough in condensed matter physics, stimulating strong interest in 2D ferroelectricity and multiferroicity. Traditional ferroelectrics/multiferroics like perovskites with large band gap and low carrier mobility are usually discussed in the 3D framework where dimensionality is not a critical issue. For a 2D van der Waals material, the ferroelectric instability thus becomes of interest, considering the fact that the size effect of ferroelectricity was once one of the central issues for the physics of ferroelectrics due to the depolarization

field [112–115]. Such depolarization field effect in a true 2D system may no longer be an issue.

For application consideration, atomically thin ferroelectrics, if any, would make ultra-high-density data storage possible. The van der Waals interaction at the interface between 2D materials and 3D semiconductors also allows lattice mismatch for epitaxial growth, while many 2D materials are already known to be semiconductors with high mobility that may become the basic materials for future wafers. Although research on 2D multiferroics is still at the early stage, and most reports are purely theoretical designs [116], the results available so far on the ME coupling in 2D systems are diversified but the scheme of ‘magnetic reading + electrical writing’ may be more easily accessed in 2D multiferroics.

It has been predicted that many 2D multiferroics are of type-I characters with independent magnetism and ferroelectricity. The covalent functionalization may induce ferroelectricity, and thus multiferroicity may be obtained by functionalization of nanomagnets. First, magnetic quasi-1D transition metal and molecule sandwiched nanowires, as shown in Fig. 8a, can also become ferroelectric via partial functionalization that can transform the sandwiched benzenes into difluorobenzene, dichlorobenzene, dicyanobenzene, etc. The broken inversion symmetry allows a horizontally switchable polarization [117]. The first 2D multiferroic proposed in 2013 was based on such an approach, as shown in Fig. 8b: half-hydrogenated graphene (graphene) was known to be ferromagnetic, and it can be ferroelectric if the hydrogen atoms are substituted by hydroxyl groups [118]. Here, the in-plane electric polarization stems from the displacement of protons as the hydroxyl groups form into a hydrogen-bonded network, which is completely independent of the magnetism induced by unpaired electrons. Another design of periodically hydroxylized graphene [119] is shown in Fig. 8b, where the graphene nanorods are divided by hydroxylized regions with two magnetic zigzag edges that are antiferromagnetically coupled. The energy degeneracy of the two spin-polarized edge states can be broken by ferroelectric polarization of the hydroxylized regions, and the polarization direction will determine which spin-channel is metallic or insulating. Similarly, CH_2OCH_3 -functionalized stanene has already been predicted to be ferroelectric [119], and another theoretical work demonstrated the coexistence of ferroelectricity and ferromagnetism in germanene that is half-side passivated by $-\text{CH}_2\text{OCH}_3$ [120]. The in-plane polarization ($\sim 0.8 \times 10^{-10} \text{ C/m}$) can be switched by a rotation of ligands with a low kinetic barrier of $\sim 0.1 \text{ eV}$, and the unoccupied

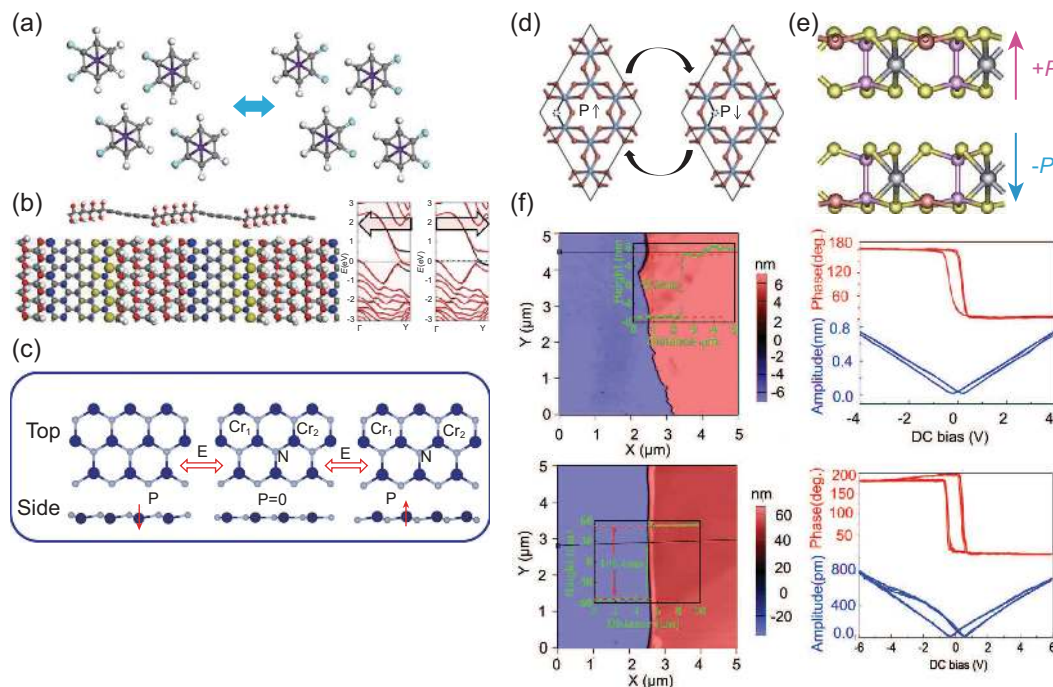


Figure 8. (a) Multiferoicity induced by partial functionalizations of ligand-like halogen on quasi-1D transition-metal-molecular-sandwich nanowires, where the polarization can be reversed upon the rotation of polar nanowires [117]. (b) Multiferoic periodically hydroxylated graphene nanorods, where the polarization of hydroxylated regions can control the spin-splitting of edge states [119]. (c) Vertical ferroelectric in magnetic CrN induced by off-centering atomic displacements of Cr atoms [121]. (d) Ferroelectric switching upon the migration of I vacancy in CrI₃ [123]. (e) Prediction of ferroelectric switching upon the off-centering displacement of Cu atoms in monolayer CuCrP₂X₆ [124], and (f) experimental measurement of the out-of-plane ferroelectricity in few-layer CuCrP₂S₆ [125].

p_z orbitals on the non-passivated Ge sites give rise to ferromagnetism with a magnetic moment of $\sim 1.0 \mu_B$ per atom.

The coexistence of 2D ferromagnetic and ferroelectric states was also predicted in buckled CrN and CrB₂, where the out-of-plane electric polarization is induced by off-centering atomic displacements of Cr atoms while the magnetism stems from the Cr atoms too, as shown in Fig. 8c [121]. Similarly, a VOCl₂ monolayer was predicted to possess a large intrinsic in-plane spontaneous polarization of 312 pC/m and stable antiferromagnetism with a Néel temperature as high as ~ 177 K [122]. The V off-center displacement that contributes to ferroelectricity can be ascribed to the pseudo Jahn–Teller distortion, while the magnetism stems from the V ion too. Additionally, the coexistence of intrinsic ferromagnetism and switchable out-of-plane polarization induced by I vacancies in CrI₃ was revealed, where I vacancies may hop between the top and bottom surfaces easily, thereby bringing about a moderate energy barrier for polarization switching [123], as shown in Fig. 8d.

Recently, multiferoicity in the transition metal thiophosphate (TMTP) family has also been predicted. For example, monolayer CuMP₂X₆ (M = Cr, V; X = S, Se) is both ferroelectric and ferro-

magnetic [124]. The out-of-plane electric polarization is induced by the Cu off-center displacement while the magnetism stems from the Cr/V atoms, as shown in Fig. 8e. Experimental observation of the out-of-plane ferroelectricity in few-layer CuCrP₂S₆ (approximately 13 nm in thickness) at room temperature was reported later; see Fig. 8f [125]. The 2D ferromagnetism of the few layers was inferred from the magnetic hysteresis of massively stacked nanosheets at 10 K.

To our knowledge at present, MXene Hf₂VC₂F₂ monolayer is one of only two reported 2D type-II multiferoics [126], where the ferroelectricity originates directly from its magnetism, as shown in Fig. 9. The non-collinear 120° Y-type spin ordering breaks the inversion symmetry and generates a polarization perpendicular to the spin helical plane. Remarkably, the estimated multiferoic transition point can be above room temperature, while its polarization is about $\sim 2.9 \times 10^{-7} \mu C/m$, much smaller than most 2D ferroelectrics. In another prediction, a combination of type-I and type-II multiferoic modes was revealed in CrOOH, where the switchable polarization was estimated to be $1300 \mu C/m^2$ [127]. The out-of-plane polarization of $1.2 \times 10^{-5} \mu C/m$ appears in a thin layer of CrOOH isolated from the (001)

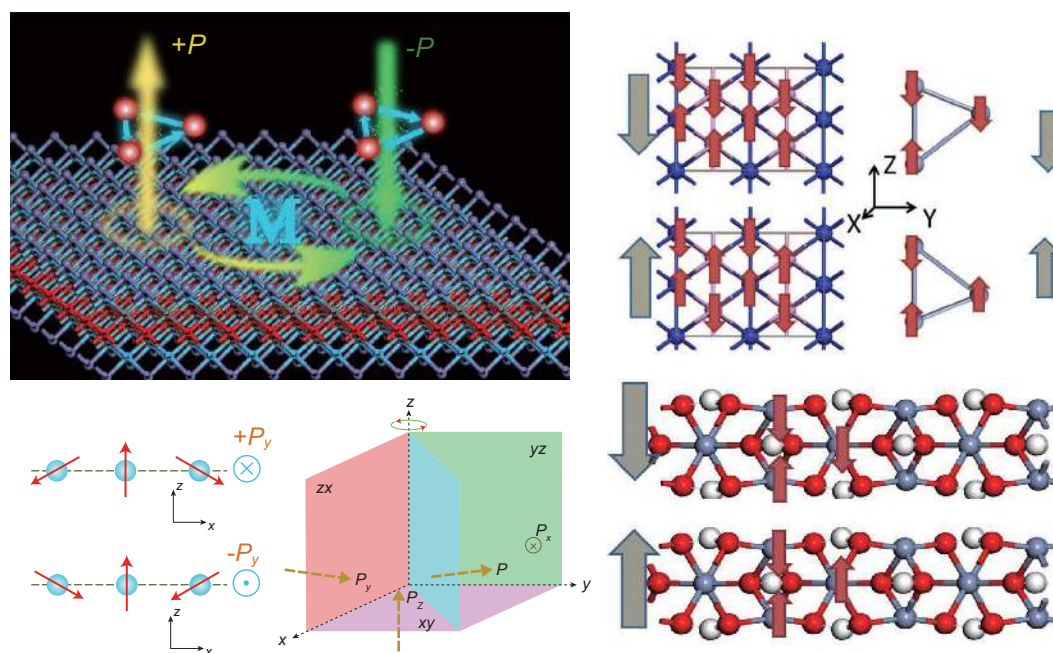


Figure 9. Type-II multiferroicity in MXene $\text{Hf}_2\text{VC}_2\text{F}_2$ monolayer [126] (left) and in bulk/thin-layer CrOOH [127] (right), where the red arrows denote spin directions and olive arrows denote polarization directions.

surface. This CrOOH layer is also ferrimagnetic with a net magnetic moment as large as $3.0 \mu_B$ per unit cell that can be reversed upon the ferroelectric polarization switching.

For many reported 2D multiferroics, ferroelectricity can be used to control the spin distribution despite it not directly stemming from magnetism. A recent theoretical study [128] predicted that the $\text{C}_6\text{N}_8\text{H}$ organic network synthesized through hydrogenation of $\text{g-C}_3\text{N}_4$ is a 2D organic multiferroic with coupled ferromagnetism and ferroelectricity. Its ferroelectricity stems from the proton-transfer within the 2D organic network, which can be used to control the magnetism as the protons make the spin-density distribution anisotropic. As shown in Fig. 10a, the spin-density distribution will be alerted by proton-transfer FE switching.

Another first-principles calculation [129] predicted the evidence of coupled ferroelectricity and ferromagnetism in halogen-intercalated phosphorene bilayer: the ‘mobile’ magnetism can be controlled by ferroelectric switching upon external electric field, exhibiting either an ‘on’ state with spin-selective and highly p -doped channels, or an ‘off’ state insulating for both spin and electron transport in the bottom layer attached by all electrodes. The out-of-plane ferroelectric polarization can be maintained against the depolarization field, rendering high-density data storage possible. Moreover, all these functionalities in the halogenated regions can be directly integrated into a 2D phosphorene wafer,

similar to the n/p channels in a doped silicon wafer. Herein the ferroelectricity is induced by halogen adatom hopping between neighboring bilayers, as shown in Fig. 10b, where the hopping from the upper layer to the lower layer will also ‘transfer’ the magnetic moment from the up state to the down state. The intercalation of halogen or hydrogen adatoms may be extended to other van der Waals bilayers like graphene for the generation of 2D out-of-plane ferroelectric polarization.

Similar ME coupling in metal-intercalated MoS_2 bilayer has been predicted. Taking $\text{Co}_{0.028}\text{MoS}_2$ as an example [130], the ferromagnetic ground state is 55 meV per unit cell lower in energy than that of the antiferromagnetic state, revealing the robust ferromagnetism at ambient conditions. During the switching from state I to state II, a net charge around $0.04e$ is transferred from the upper layer to the lower layer. The upper layer is mostly spin non-polarized when the electrical polarization points downwards in state I, but becomes spin polarized as the polarization is reversed into state II, and vice versa for the lower layer, as marked by the spin densities in Fig. 10c. As a result, the ferroelectricity and magnetism can be coupled, where the spin distribution can be controlled by the electric field, rendering efficient ‘magnetic reading + electrical writing’.

There have also been reports that the net magnetization of 2D multiferroics can be reversed by ferroelectric switching. When a metal porphyrin (MP) molecule is intercalated between two CrI_3 layers, the

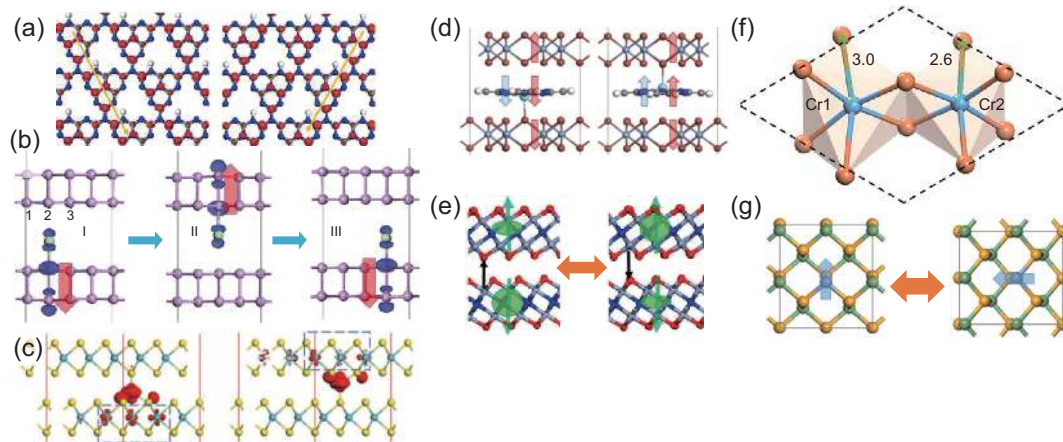


Figure 10. The change of magnetic distribution (in red or blue) upon ferroelectric switching in 2D multiferroics: (a) C_6N_8H organic network [128], (b) hydrogen/halogen intercalated 2D van der Waals bilayer [129], and (c) Co-intercalated bilayer MoS_2 [130]; reversal of net magnetization upon ferroelectric switching in 2D multiferroics: (d) MP intercalated bilayer CrI_3 , [131] and (e) bilayer MXene, VS_2 , and MoN_2 [132]; the change of magnetic easy axis upon (f) 120 degree ferroelectric switching in charged $CrBr_3$ monolayer [133] and (g) 90 degree ferroelectric switching in Cr-doped GeSe monolayer [134].

metal ion will be bound to either side [131]. As a result, a double-well potential can be created, which gives rise to a switchable out-of-plane polarization of ~ 0.08 eÅ with the barrier lower than 0.35 eV. Since CrI_3 has been verified to be intralayer ferromagnetic and interlayer antiferromagnetic, the net magnetization of bilayer CrI_3 should be zero. Upon the intercalation of magnetic MP molecules, however, both TiP/VP will be ferromagnetically coupled to the binding layer. Each TiP and VP molecule possesses a magnetic moment of $\sim 2.0 \mu_B$ and $\sim 3.0 \mu_B$, respectively, and the intercalated bilayer systems keeps the same net magnetization, which can be reversed as the MP binding to the other side upon ferroelectric switching, as displayed in Fig. 10d.

In another work, a series of van der Waals bilayers (BN, MoS_2 , etc.) have been predicted to be 2D ferroelectrics with an interlayer voltage [132], while some magnetic bilayers such as MXenes, VS_2 , MoN_2 , and $LaCl/LaBr$ are multiferroic. For two monolayers that are antiferromagnetically coupled in the ground state, which are inequivalent due to the interlayer charge transfer and voltage difference, their total magnetic moments may be a non-zero value upon an incomplete compensation. The total magnetization can be switched with the reversal of polarization and interlayer voltage, as shown in Fig. 10e, and the predicted switchable magnetizations for bilayer MXene, VS_2 , and MoN_2 are respectively 0.008, 0.016, and $0.09 \mu_B$ per unit cell.

In some 2D multiferroics where the easy axis of magnetism is coupled with the electric polarization direction, the magnetization may rotate by an angle as the ferroelectric polarization switches to another axis. A first-principles study [133] revealed that a

charged $CrBr_3$ monolayer exhibits the in-plane multiferroicity with coexisting ferromagnetism and ferroelectricity, which is ensured by the combination of orbital and charge ordering as realized by the asymmetric Jahn–Teller distortions of octahedral $Cr - Br_6$ units, as displayed in Fig. 10f. The easy axis of magnetization is within the atomic plane and parallel to the in-plane polarization, so the magnetization will be switched by 120 degrees upon a 120 degree ferroelectric switching. In another study [134], 2D triferroics (ferroelectricity + ferromagnetism + ferroelasticity) can even be obtained by doping 3d transition metal ions in group-IV monochalcogenide monolayers, which were previously revealed to be ferroelastic multiferroics [135,136]. For some Cr-doped systems including (Cr)SnS, (Cr)GeSe, and (Cr)SnSe, their easy axis of magnetization is aligned along the x -axis in-plane, which will switch to the y -axis upon either ferroelastic switching or 90 degree FE switching due to the swapping of zigzag and armchair direction, and vice versa if the easy axis is aligned along the y -axis, as displayed in Fig. 10g. As a result, upon ferroelastic switching or 90 degree FE switching, their magnetization direction will also switch by 90 degrees, so the ferromagnetism, ferroelectricity, and ferroelasticity are all coupled for efficient data reading and writing.

FINAL REMARKS

To summarize, we have presented a brief overview on the recent progress of single-phase multiferroics, and it is shown that multiferroicity is still one of the hottest topics in condensed matter physics and materials sciences. Given the rapidly developing

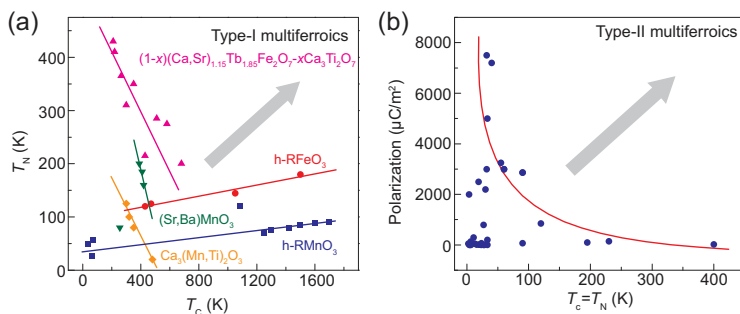


Figure 11. A brief summary of physical properties such as Néel point T_N , ferroelectric transition T_C , and polarization for (a) type-I and (b) type-II multiferroics. In (a), the listed materials show a common feature that the magnetic cation is essentially involved in generating ferroelectricity. In (b), ferroelectric polarization is roughly inversely proportional to $T_C (= T_N)$ in type-II multiferroics. The gray arrows in both (a) and (b) indicate the target of multiferroic research.

nature of this discipline and the authors' personal bias, it is inevitable that some important papers on this topic have been missed in the present review. In the past five years, tremendous progress has been made in understanding materials chemistry, multiferroicity, and ME coupling. However, the search for new multiferroic materials with good properties, i.e. high temperature, large polarization, strong magnetization, and significant ME coupling, is still underway.

As illustrated in Fig. 11, developed based on our collection of available data, it is clear where the way is for our further efforts (large arrows) while the as-shown dependences are intrinsic in physics. For type-I multiferroics, both T_C and T_N can be above room temperature, and electric polarization can reach $\sim 10 \mu\text{C}/\text{cm}^2$ or even larger. However, the ME response is usually weak without much exception. For type-II multiferroics, the remarkable ME coupling cannot prevent our disappointment at the weak ferroelectricity and ferromagnetism. Therefore, to approach the upper-right corners of the diagrams, we need a distinctly different and more promising strategy in single-phase multiferroics.

In comparison with ferroelectricity, magnetism such as net magnetization and T_N looks much harder to improve in all types of multiferroics. Note that the existence of large macroscopic magnetization is critical for electro-control of magnetism. Regarding this, multiferroics containing more than one type of magnetic moments (due to different elements/valent states/sites etc.) deserve special attention. These various magnetic moments can form either clusters (blocks) or a ferrimagnetic configuration, and thus may allow remarkable macroscopic magnetization without damaging the ferroelectric state, as exemplified in the hexaferrites and the $(\text{Mn}, \text{Fe})_2\text{Mo}_3\text{O}_8$ family [62,81]. This scenario is not only expected in type-II multiferroics, but also looks compatible with type-I multiferroics, especially for

those double-layered perovskites showing hybrid improper multiferroicity. An impressive detail of the hybrid mechanism in orthorhombic RMnO_3 is the existence of R and Mn, both of which are magnetic, parallel to the scenario proposed to enhance magnetization in multiferroics. Regarding T_N , it is another roadblock. Even for type-I multiferroics, most of them have low T_N below room temperature. Nevertheless, several routes to enhance T_N include at least two aspects. First, Fe-based multiferroics usually have a relatively higher T_N than manganites, probably due to the stronger Fe–Fe exchange [30]. Second, the tolerance factor is pivotal in tuning T_N in multiferroics, as exemplified in both h-RMnO_3 and RFeO_3 [38]. In fact, it was recently found that the tolerance factor has a considerable impact on the properties in double-layered perovskites [94].

Apart from these focused issues, emergent phenomena such as non-reciprocity, giant thermal Hall effect, and topological domain structure are indeed appealing, and have largely broadened the conception of multiferroicity and may bring new functionalities of multiferroics. While these phenomena show fascinating aspects, one may wonder how these effects could be coupled to the various ferroic orders. Furthermore, more emergent and interesting properties hosted in a multiferroic await exploration, and thus certainly more extensive investigations are required to explore the full merit of multiferroics, paving the way for multiferroic research into a new era.

FUNDING

This work was supported by the National Nature Science Foundation of China (11774106, 51431006, 21573084, 11834002, 51721001 and 11874031) and the National Key Research Projects of China (2016YFA0300101).

REFERENCES

- Schmid H. Multi-ferroic magnetoelectrics. *Ferroelectrics* 1994; **162**: 317–38.
- Kimura T, Goto T and Shintani H et al. Magnetic control of ferroelectric polarization. *Nature* 2003; **426**: 55–8.
- Wang J, Neaton JB and Zheng Het al. Epitaxial BiFeO_3 multiferroic thin film heterostructures. *Science* 2003; **299**: 1719–22.
- Khomskii D. Classifying multiferroics: mechanisms and effects. *Physics* 2009; **2**: 20.
- Benedek NA and Fennie CJ. Hybrid improper ferroelectricity: a mechanism for controllable polarization-magnetization coupling. *Phys Rev Lett* 2011; **106**: 107204.
- Oh YS, Luo X and Huang FT et al. Experimental demonstration of hybrid improper ferroelectricity and the presence of abundant charged walls in $(\text{Ca}, \text{Sr})_3\text{Ti}_2\text{O}_7$ crystals. *Nat Mater* 2015; **14**: 407–13.

7. Yang Y, Xiang H and Zhao H *et al*. Improper ferroelectricity at antiferromagnetic domain walls of perovskite oxides. *Phys Rev B* 2017; **96**: 104431.
8. Cheong S-W, Talbayev D and Kiryukhin V *et al*. Broken symmetries, non-reciprocity, and multiferroicity. *npj Quantum Mater* 2018; **3**: 19.
9. Tokura Y and Nagaosa N. Nonreciprocal responses from non-centrosymmetric quantum materials. *Nat Commun* 2018; **9**: 3740.
10. Huang F-T and Cheong S-W. Aperiodic topological order in the domain configurations of functional materials. *Nat Rev Mater* 2017; **2**: 17004.
11. Ideue T, Kurumaji T and Ishiwata S *et al*. Giant thermal Hall effect in multiferroics. *Nat Mater* 2017; **16**: 797–802.
12. Dong S, Liu J-M and Cheong S-W *et al*. Multiferroic materials and magneto-electric physics: symmetry, entanglement, excitation, and topology. *Adv Phys* 2015; **64**: 519–626.
13. Cheong S-W and Mostovoy M. Multiferroics: a magnetic twist for ferroelectricity. *Nat Mater* 2007; **6**: 13–20.
14. Tokura Y and Seki S. Multiferroics with spiral spin orders. *Adv Mater* 2010; **22**: 1554–65.
15. Lu C, Hu W and Tian Y *et al*. Multiferroic oxide thin films and heterostructures. *Appl Phys Rev* 2015; **2**: 021304.
16. Spaldin NA and Ramesh R. Advances in magnetoelectric multiferroics. *Nat Mater* 2019; **18**: 203–12.
17. Belik AA. Polar and nonpolar phases of BiMO₃: a review. *J Solid State Chem* 2012; **195**: 32–40.
18. Lee JH, Fang L and Vlahos E *et al*. A strong ferroelectric ferromagnet created by means of spin-lattice coupling. *Nature* 2010; **466**: 954–8.
19. Aken BBV, Palstra TT and Filippetti A *et al*. The origin of ferroelectricity in magnetoelectric YMnO₃. *Nat Mater* 2004; **3**: 164–70.
20. Fiebig M, Lottermoser T and Frohlich D *et al*. Observation of coupled magnetic and electric domains. *Nature* 2002; **419**: 818–20.
21. Choi T, Horibe Y and Yi HT *et al*. Insulating interlocked ferroelectric and structural antiphase domain walls in multiferroic YMnO₃. *Nat Mater* 2010; **9**: 253–8.
22. Geng Y, Das H and Wysocki AL *et al*. Direct visualization of magnetoelectric domains. *Nat Mater* 2014; **13**: 163–7.
23. Yang KL, Zhang Y and Zheng SH *et al*. Electric field driven evolution of topological domain structure in hexagonal manganites. *Phys Rev B* 2017; **96**: 144103.
24. Han MG, Zhu Y and Wu L *et al*. Ferroelectric switching dynamics of topological vortex domains in a hexagonal manganite. *Adv Mater* 2013; **25**: 2415–21.
25. Yang KL, Zhang Y and Zheng SH *et al*. Spatial anisotropy of topological domain structure in hexagonal manganites. *Phys Rev B* 2017; **95**: 024114.
26. Wang X, Huang F-T and Hu R *et al*. Self-poling with oxygen off-stoichiometry in ferroelectric hexagonal manganites. *APL Mater* 2015; **3**: 041505.
27. Pang H, Zhang F and Zeng M *et al*. Preparation of epitaxial hexagonal YMnO₃ thin films and observation of ferroelectric vortex domains. *npj Quantum Mater* 2016; **1**: 16015.
28. Cheng S, Li J and Han MG *et al*. Topologically allowed nonsixfold vortices in a sixfold multiferroic material: observation and classification. *Phys Rev Lett* 2017; **118**: 145501.
29. Li Y, Jin Y and Lu X *et al*. Rewritable ferroelectric vortex pairs in BiFeO₃. *npj Quantum Mater* 2017; **2**: 43.
30. Xu X and Wang W. Multiferroic hexagonal ferrites (h-RFeO₃, R = Y, Dy-Lu): a brief experimental review. *Mod Phys Lett B* 2014; **28**: 1430008.
31. Das H, Wysocki AL and Geng Y *et al*. Bulk magnetoelectricity in the hexagonal manganites and ferrites. *Nat Commun* 2014; **5**: 2998.
32. Wang W, Zhao J and Wang W *et al*. Room-temperature multiferroic hexagonal LuFeO₃ films. *Phys Rev Lett* 2013; **110**: 237601.
33. Han H, Kim D and Chae S *et al*. Switchable ferroelectric photovoltaic effects in epitaxial h-RFeO₃ thin films. *Nanoscale* 2018; **10**: 13261–9.
34. Han H, Kim D and Chu K *et al*. Enhanced switchable ferroelectric photovoltaic effects in hexagonal ferrite thin films via strain engineering. *ACS Appl Mater Interfaces* 2018; **10**: 1846–53.
35. Lin L, Zhang HM and Liu MF *et al*. Hexagonal phase stabilization and magnetic orders of multiferroic Lu_{1-x}Sc_xFeO₃. *Phys Rev B* 2016; **93**: 075146.
36. Du K, Gao B and Wang Y *et al*. Vortex ferroelectric domains, large-loop weak ferromagnetic domains, and their decoupling in hexagonal (Lu,Sc)FeO₃. *npj Quantum Mater* 2018; **3**: 33.
37. Disseler SM, Luo X and Gao B *et al*. Multiferroicity in doped hexagonal LuFeO₃. *Phys Rev B* 2015; **92**: 054435.
38. Sinha K, Wang H and Wang X *et al*. Tuning the Neel temperature of hexagonal ferrites by structural distortion. *Phys Rev Lett* 2018; **121**: 237203.
39. Garcia-Castro AC, Ibarra-Hernandez W and Bousquet E *et al*. Direct magnetization-polarization coupling in BaCuF₄. *Phys Rev Lett* 2018; **121**: 117601.
40. Ederer C and Spaldin NA. Origin of ferroelectricity in the multiferroic barium fluorides BaMF₄: a first principles study. *Phys Rev B* 2006; **74**: 024102.
41. Scott JF and Blinc R. Multiferroic magnetoelectric fluorides: why are there so many magnetic ferroelectrics? *J Phys Condens Matter* 2011; **23**: 113202.
42. Zhou S, Weng Y and Wu Z *et al*. Strong room-temperature blue-violet photoluminescence of multiferroic BaMnF₄. *Phys Chem Chem Phys* 2016; **18**: 2054–8.
43. Hur N, Park S and Sharma PA *et al*. Electric polarization reversal and memory in a multiferroic material induced by magnetic fields. *Nature* 2004; **429**: 392–5.
44. Picozzi S, Yamauchi K and Sanyal B *et al*. Dual nature of improper ferroelectricity in a magnetoelectric multiferroic. *Phys Rev Lett* 2007; **99**: 227201.
45. Sergienko IA, Sen C and Dagotto E. Ferroelectricity in the magnetic E-phase of orthorhombic perovskites. *Phys Rev Lett* 2006; **97**: 227204.
46. Aoyama T, Yamauchi K and Iyama A *et al*. Giant spin-driven ferroelectric polarization in TbMnO₃ under high pressure. *Nat Commun* 2014; **5**: 4927.
47. Aupiais I, Mochizuki M and Sakata H *et al*. Colossal electromagnon excitation in the non-cycloidal phase of TbMnO₃ under pressure. *npj Quantum Mater* 2018; **3**: 60.
48. Aoyama T, Iyama A and Shimizu K *et al*. Multiferroicity in orthorhombic RMnO₃ (R = Dy, Tb, and Gd) under high pressure. *Phys Rev B* 2015; **91**: 081107.
49. Murakawa H, Onose Y and Miyahara S *et al*. Ferroelectricity induced by spin-dependent metal-ligand hybridization in Ba₂CoGe₂O₇. *Phys Rev Lett* 2010; **105**: 137202.
50. Ghara S, Suard E and Fauth F *et al*. Ordered aeschynite-type polar magnets RFeWO₆ (R = Dy, Eu, Tb, and Y): a new family of type-II multiferroics. *Phys Rev B* 2017; **95**: 224416.
51. Liu M, Lin L and Zhang Y *et al*. Cycloidal magnetism driven ferroelectricity in double tungstate LiFe(WO₄)₂. *Phys Rev B* 2017; **95**: 195134.
52. Chen R, Wang JF and Ouyang ZW *et al*. Magnetic field induced ferroelectricity and half magnetization plateau in polycrystalline R₂V₂O₇ (R = Ni, Co). *Phys Rev B* 2018; **98**: 184404.
53. Liu YJ, Wang JF and He ZZ *et al*. Unusual magnetoelectric memory and polarization reversal in the kagome staircase compound Ni₃V₂O₈. *Phys Rev B* 2018; **97**: 174429.
54. Nojiri H, Yoshii S and Yasui M *et al*. Neutron Laue diffraction study on the magnetic phase diagram of multiferroic MnWO₄ under pulsed high magnetic fields. *Phys Rev Lett* 2011; **106**: 237202.
55. Terada N, Ikedo Y and Sato H *et al*. Rich magnetoelectric phase diagrams of multiferroic single-crystal α-NaFeO₂. *Phys Rev B* 2017; **96**: 035128.

56. Cong J, Zhai K and Chai Y *et al.* Spin-induced multiferroicity in the binary perovskite manganite Mn_2O_3 . *Nat Commun* 2018; **9**: 2996.
57. Zhou L, Dai J and Chai Y *et al.* Realization of large electric polarization and strong magnetoelectric coupling in $\text{BiMn}_3\text{Cr}_4\text{O}_{12}$. *Adv Mater* 2017; **29**: 1703435.
58. Wang X, Chai Y and Zhou L *et al.* Observation of magnetoelectric multiferroicity in a cubic perovskite system: $\text{LaMn}_3\text{Cr}_4\text{O}_{12}$. *Phys Rev Lett* 2015; **115**: 087601.
59. Oh YS, Artyukhin S and Yang JJ *et al.* Non-hysteretic colossal magnetoelectricity in a collinear antiferromagnet. *Nat Commun* 2014; **5**: 3201.
60. Cai G-H, Greenblatt M and Li M-R. Polar magnets in double corundum oxides. *Chem Mater* 2017; **29**: 5447–57.
61. Wang Y, Pascut GL and Gao B *et al.* Unveiling hidden ferrimagnetism and giant magnetoelectricity in polar magnet $\text{Fe}_2\text{Mo}_3\text{O}_8$. *Sci Rep* 2015; **5**: 12268.
62. Kurumaji T, Ishiwata S and Tokura Y. Diagonal magnetoelectric susceptibility and effect of Fe doping in the polar ferrimagnet $\text{Mn}_2\text{Mo}_3\text{O}_8$. *Phys Rev B* 2017; **95**: 045142.
63. Kurumaji T, Ishiwata S and Tokura Y. Doping-tunable ferrimagnetic phase with large linear magnetoelectric effect in a polar magnet $\text{Fe}_2\text{Mo}_3\text{O}_8$. *Phys Rev X* 2015; **5**: 031034.
64. Khanh ND, Abe N and Sagayama H *et al.* Magnetoelectric coupling in the honeycomb antiferromagnet $\text{Co}_4\text{Nb}_2\text{O}_9$. *Phys Rev B* 2016; **93**: 075117.
65. Li MR, McCabe EE and Stephens PW *et al.* Magnetostriction-polarization coupling in multiferroic Mn_2MnWO_6 . *Nat Commun* 2017; **8**: 2037.
66. Klimin SA, Kuzmenko AB and Kashchenko MA *et al.* Infrared study of lattice dynamics and spin-phonon and electron-phonon interactions in multiferroic $\text{TbFe}_3(\text{BO}_3)_4$ and $\text{GdFe}_3(\text{BO}_3)_4$. *Phys Rev B* 2016; **93**: 054304.
67. Popova MN, Malkin BZ and Boldyrev KN *et al.* Evidence for a collinear easy-plane magnetic structure of multiferroic $\text{EuFe}_3(\text{BO}_3)_4$: apectroscopic and theoretical studies. *Phys Rev B* 2016; **94**: 184418.
68. Hayashida S, Asai S and Kato D *et al.* Magnetic order in the rare-earth ferromagnet $\text{CeFe}_3(\text{BO}_3)_4$. *Phys Rev B* 2018; **98**: 224405.
69. Nilsen GJ, Simonet V and Colin CV *et al.* Phase diagram of multiferroic $\text{KCu}_3\text{As}_2\text{O}_7(\text{OD})_3$. *Phys Rev B* 2017; **95**: 214415.
70. Baum M, Komarek AC and Holbein S *et al.* Magnetic structure and multiferroic coupling in pyroxene $\text{NaFeSi}_2\text{O}_6$. *Phys Rev B* 2015; **91**: 214415.
71. Terada N, Khalyavin DD and Manuel P *et al.* Ferroelectricity induced by ferriaxial crystal rotation and spin helicity in a B-site-ordered double-perovskite multiferroic $\text{In}_2\text{NiMnO}_6$. *Phys Rev B* 2015; **91**: 104413.
72. Zhang Y, Lin L and Zhang J-J *et al.* Exchange striction driven magnetodielectric effect and potential photovoltaic effect in polar CaOFeS . *Phys Rev Mater* 2017; **1**: 034406.
73. De C, Ter-Oganessian NV and Sundaresan A. Spin-driven ferroelectricity and large magnetoelectric effect in monoclinic MnSb_2S_4 . *Phys Rev B* 2018; **98**: 174430.
74. Dong S, Liu JM and Dagotto E. BaFeSe : a high T_C magnetic multiferroic with large ferrielectric polarization. *Phys Rev Lett* 2014; **113**: 187204.
75. Wu HC, Chandrasekhar KD and Yuan JK *et al.* Anisotropic spin-flip-induced multiferroic behavior in kagome $\text{Cu}_3\text{Bi}(\text{SeO}_3)_2\text{O}_2\text{Cl}$. *Phys Rev B* 2017; **95**: 125121.
76. Miyake A, Shibuya J and Akaki M *et al.* Magnetic field induced polar phase in the chiral magnet CsCuCl_3 . *Phys Rev B* 2015; **92**: 100406.
77. Zhao L, Hung TL and Li CC *et al.* CuBr_2 : a new multiferroic material with high critical temperature. *Adv Mater* 2012; **24**: 2469–73.
78. Lin L, Xie YL and Wen JJ *et al.* Experimental observation of magnetoelectricity in spin ice $\text{Dy}_2\text{Ti}_2\text{O}_7$. *New J Phys* 2015; **17**: 123018.
79. Liu D, Lin L and Liu MF *et al.* Multiferroicity in spin ice $\text{Ho}_2\text{Ti}_2\text{O}_7$: an investigation on single crystals. *J Appl Phys* 2013; **113**: 17D901.
80. Xu Z-C, Liu M-F and Lin L *et al.* Experimental observations of ferroelectricity in double pyrochlore $\text{Dy}_2\text{Ru}_2\text{O}_7$. *Front Phys* 2013; **9**: 82–9.
81. Zhai K, Wu Y and Shen S *et al.* Giant magnetoelectric effects achieved by tuning spin cone symmetry in Y-type hexaferrites. *Nat Commun* 2017; **8**: 519.
82. Zhao HJ, Ren W and Yang Y *et al.* Near room-temperature multiferroic materials with tunable ferromagnetic and electrical properties. *Nat Commun* 2014; **5**: 4021.
83. Lu C, Dong S and Xia Z *et al.* Polarization enhancement and ferroelectric switching enabled by interacting magnetic structures in DyMnO_3 thin films. *Sci Rep* 2013; **3**: 3374.
84. Lu C and Liu J-M. DyMnO_3 : a model system of type-II multiferroics. *J Materials* 2016; **2**: 213–24.
85. Lu C, Deniz H and Li X *et al.* Continuous magnetoelectric control in multiferroic DyMnO_3 films with twin-like domains. *Sci Rep* 2016; **6**: 20175.
86. Hu N, Lu C and Xia Z *et al.* Multiferroicity and magnetoelectric coupling in TbMnO_3 thin films. *ACS Appl Mater Interfaces* 2015; **7**: 26603–7.
87. Li X, Lu C and Dai J *et al.* Novel multiferroicity in GdMnO_3 thin films with self-assembled nano-twinned domains. *Sci Rep* 2014; **4**: 7019.
88. Wang HW, Li CL and Yuan SL *et al.* The crucial role of Mn spiral spin order in stabilizing the Dy-Mn exchange striction in multiferroic DyMnO_3 . *Phys Chem Chem Phys* 2017; **19**: 3706–12.
89. Toyoda S, Abe N and Kimura S *et al.* One-way transparency of light in multiferroic CuB_2O_4 . *Phys Rev Lett* 2015; **115**: 267207.
90. Toyoda S, Abe N and Arima T. Gigantic directional asymmetry of luminescence in multiferroic CuB_2O_4 . *Phys Rev B* 2016; **93**: 201109.
91. Yu S, Gao B and Kim JW *et al.* High-temperature terahertz optical diode effect without magnetic order in polar $\text{FeZnMo}_3\text{O}_8$. *Phys Rev Lett* 2018; **120**: 037601.
92. Kezsmarki I, Nagel U and Bordacs S *et al.* Optical diode effect at spin-wave excitations of the room-temperature multiferroic BiFeO_3 . *Phys Rev Lett* 2015; **115**: 127203.
93. Iguchi Y, Nii Y and Onose Y. Magneto-electrical control of nonreciprocal microwave response in a multiferroic helimagnet. *Nat Commun* 2017; **8**: 15252.
94. Liu XQ, Chen BH and Lu JJ *et al.* Hybrid improper ferroelectricity in B-site substituted $\text{Ca}_3\text{Ti}_2\text{O}_7$: the role of tolerance factor. *Appl Phys Lett* 2018; **113**: 242904.
95. Gao B, Huang F-T and Wang Y *et al.* Interrelation between domain structures and polarization switching in hybrid improper ferroelectric $\text{Ca}_3(\text{Mn,Ti})_2\text{O}_7$. *Appl Phys Lett* 2017; **110**: 222906.
96. Liu M, Zhang Y and Lin L-F *et al.* Direct observation of ferroelectricity in $\text{Ca}_3\text{Mn}_2\text{O}_7$ and its prominent light absorption. *Appl Phys Lett* 2018; **113**: 022902.
97. Pitcher MJ, Mandal P and Dyer MS *et al.* Tilt engineering of spontaneous polarization and magnetization above 300 K in a bulk layered perovskite. *Science* 2015; **347**: 420.
98. Li X, Yang L and Li CF *et al.* Ultra-low coercive field of improper ferroelectric $\text{Ca}_3\text{Ti}_2\text{O}_7$ epitaxial thin films. *Appl Phys Lett* 2017; **110**: 042901.
99. Rondinelli JM, Eidelson AS and Spaldin NA. Non- d^0 Mn-driven ferroelectricity in antiferromagnetic BaMnO_3 . *Phys Rev B* 2009; **79**: 205119.
100. Sakai H, Fujioka J and Fukuda T *et al.* Displacement-type ferroelectricity with off-center magnetic ions in perovskite $\text{Sr}_{1-x}\text{Ba}_x\text{MnO}_3$. *Phys Rev Lett* 2011; **107**: 137601.
101. Guo JW, Wang PS and Yuan Y *et al.* Strain-induced ferroelectricity and spin-lattice coupling in SrMnO_3 thin films. *Phys Rev B* 2018; **97**: 235135.

102. Edström A and Ederer C. First-principles-based strain and temperature-dependent ferroic phase diagram of SrMnO₃. *Phys Rev Mater* 2018; **2**: 104409.
103. Chen H and Millis AJ. Phase diagram of Sr_{1-x}Ba_xMnO₃ as a function of chemical doping, epitaxial strain, and external pressure. *Phys Rev B* 2016; **94**: 165106.
104. Bayaraa T, Yang Y and Zhao HJ *et al*. Structural and magnetic transitions accompanied by large responses in epitaxial Sr_{0.5}Ba_{0.5}MnO₃ films. *Phys Rev Mater* 2018; **2**: 084404.
105. Zhang JX, He Q and Trassin M *et al*. Microscopic origin of the giant ferroelectric polarization in tetragonal-like BiFeO₃. *Phys Rev Lett* 2011; **107**: 147602.
106. Lu C-L, Liu J-M and Wu T. Electric field driven phase transition and possible twinning quasi-tetragonal phase in compressively strained BiFeO₃ thin films. *Front Phys* 2012; **7**: 424–8.
107. Yin LH, Shi TF and Zhang RR *et al*. Electric dipoles via Cr³⁺(d³) ion off-center displacement in perovskite DyCrO₃. *Phys Rev B* 2018; **98**: 054301.
108. Indra A, Dey K and Dey JK *et al*. CrO₄ distortion-driven ferroelectric order in (R,Y)CrO₄(R = Sm,Gd,and Ho): a new family of multiferroics. *Phys Rev B* 2018; **98**: 014408.
109. Xu K, Feng JS and Liu ZP *et al*. Origin of ferrimagnetism and ferroelectricity in room-temperature multiferroic ε-Fe₂O₃. *Phys Rev Appl* 2018; **9**: 044011.
110. Kang TK, Roh CJ and Lim J *et al*. A room-temperature ferroelectric ferromagnet in a 1D tetrahedral chain network. *Adv Mater* 2019; **31**: 1808104.
111. Li X, Zheng S and Tian L *et al*. Unusual tunability of multiferroicity in GdMn₂O₅ by electric field poling far above multiferroic ordering point. *Chin Phys B* 2019; **28**: 027502.
112. Sai N, Kolpak AM and Rappe AM. Ferroelectricity in ultrathin perovskite films. *Phys Rev B* 2005; **72**: 020101.
113. Setter N, Damjanovic D and Eng L *et al*. Ferroelectric thin films: review of materials, properties, and applications. *J Appl Phys* 2006; **100**: 051606.
114. Junquera J and Ghosez P. Critical thickness for ferroelectricity in perovskite ultrathin films. *Nature* 2003; **422**: 506–9.
115. Fong DD, Stephenson GB and Streiffer SK *et al*. Ferroelectricity in ultrathin perovskite films. *Science* 2004; **304**: 1650–3.
116. Wu M and Jena P. The rise of two-dimensional van der Waals ferroelectrics. *Wiley Interdiscip Rev Comput Mol Sci* 2018; **8**: e1365.
117. Wu M, Burton JD and Tsymbal EY *et al*. Multiferroic materials based on organic transition-metal molecular nanowires. *J Am Chem Soc* 2012; **134**: 14423–9.
118. Wu M, Burton JD and Tsymbal EY *et al*. Hydroxyl-decorated graphene systems as candidates for organic metal-free ferroelectrics, multiferroics, and high-performance proton battery cathode materials. *Phys Rev B* 2013; **87**: 081406.
119. Wu M, Dong S and Yao K *et al*. Ferroelectricity in covalently functionalized two-dimensional materials: integration of high-mobility semiconductors and nonvolatile memory. *Nano Lett* 2016; **16**: 7309–15.
120. Kou L, Ma Y and Liao T *et al*. Multiferroic and ferroic topological order in ligand-functionalized germanene and arsenene. *Phys Rev Appl* 2018; **10**: 024043.
121. Luo W, Xu K and Xiang H. Two-dimensional hyperferroelectric metals: a different route to ferromagnetic-ferroelectric multiferroics. *Phys Rev B* 2017; **96**: 235415.
122. Ai H, Song X and Qi S *et al*. Intrinsic multiferroicity in two-dimensional VOCl₂ monolayers. *Nanoscale* 2019; **11**: 1103–10.
123. Zhao Y, Lin L and Zhou Q *et al*. Surface vacancy-induced switchable electric polarization and enhanced ferromagnetism in monolayer metal trihalides. *Nano Lett* 2018; **18**: 2943–9.
124. Qi J, Wang H and Chen X *et al*. Two-dimensional multiferroic semiconductors with coexisting ferroelectricity and ferromagnetism. *Appl Phys Lett* 2018; **113**: 043102.
125. Lai Y, Song Z and Wan Y *et al*. Two-dimensional ferromagnetism and driven ferroelectricity in van der Waals CuCrP₂S₆. *Nanoscale* 2019; **11**: 5163–70.
126. Zhang J-J, Lin L and Zhang Y *et al*. Type-II multiferroic Hf₂VC₂F₂ MXene monolayer with high transition temperature. *J Am Chem Soc* 2018; **140**: 9768–73.
127. Wu M, Duan T and Lu C *et al*. Proton transfer ferroelectricity/multiferroicity in rutile oxyhydroxides. *Nanoscale* 2018; **10**: 9509–15.
128. Tu Z, Wu M and Zeng XC. Two-dimensional metal-free organic multiferroic material for design of multifunctional integrated circuits. *J Phys Chem Lett* 2017; **8**: 1973–8.
129. Yang Q, Xiong W and Zhu L *et al*. Chemically functionalized phosphorene: two-dimensional multiferroics with vertical polarization and mobile magnetism. *J Am Chem Soc* 2017; **139**: 11506–12.
130. Tu Z and Wu M. 2D diluted multiferroic semiconductors upon intercalation. *Adv Electron Mater* 2019; **6**: 1800960.
131. Yang Q, Zhong T and Tu Z *et al*. Design of single-molecule multiferroics for efficient ultrahigh-density nonvolatile memories. *Adv Sci* 2019; **6**: 1801572.
132. Li L and Wu M. Binary compound bilayer and multilayer with vertical polarizations: two-dimensional ferroelectrics, multiferroics, and nanogenerators. *ACS Nano* 2017; **11**: 6382–8.
133. Huang C, Du Y and Wu H *et al*. Prediction of intrinsic ferromagnetic ferroelectricity in a transition-metal halide monolayer. *Phys Rev Lett* 2018; **120**: 147601.
134. Yang L, Wu M and Yao K. Transition-metal-doped group-IV monochalcogenides: a combination of two-dimensional triferroics and diluted magnetic semiconductors. *Nanotechnology* 2018; **29**: 215703.
135. Wu M and Zeng XC. Intrinsic ferroelasticity and/or multiferroicity in two-dimensional phosphorene and phosphorene analogues. *Nano Lett* 2016; **16**: 3236–41.
136. Wu M and Zeng XC. Bismuth oxychalcogenides: a new class of ferroelectric/ferroelastic materials with ultra high mobility. *Nano Lett* 2017; **17**: 6309–14.